Observation of the Magnon Hall Effect

Y. Onose,[1,2]* T. Ideue,[1] H. Katsura,[3] Y. Shiomi,[1,4] N. Nagaosa,[1,4] Y. Tokura[1,2,4]

The Hall effect usually occurs in conductors when the Lorentz force acts on a charge current in the presence of a perpendicular magnetic field. Neutral quasi-particles such as phonons and spins can, however, carry heat current and potentially exhibit the thermal Hall effect without resorting to the Lorentz force. We report experimental evidence for the anomalous thermal Hall effect caused by spin excitations (magnons) in an insulating ferromagnet with a pyrochlore lattice structure. Our theoretical analysis indicates that the propagation of the spin waves is influenced by the Dzyaloshinskii-Moriya spin-orbit interaction, which plays the role of the vector potential, much as in the intrinsic anomalous Hall effect in metallic ferromagnets.

Electronics based on the spin degree of freedom (spintronics) may lead to developments beyond silicon-based technologies (*1*); spintronics avoids the dissipation from Joule heating by replacing charge currents with currents of the magnetic moment (spin currents). Phenomena such as the spin Hall effect (generation of a transverse spin current by a longitudinal electric field) in metals and semiconductors have therefore recently attracted much attention (*2*). However, some dissipation is still inevitable because the spin current in these conducting materials is carried by electronic carriers. In this sense, achieving spin transport in insulating magnets may be more promising.

In magnetic insulators, the spin moments are carried by magnons, which are quanta of magnetic excitations. A fundamental question for the magnon spin current is whether it exhibits the Hall effect, which is usually driven by the Lorentz force; therefore, charge-free particles (such as photons, phonons, and magnons) may be expected not to lead to it. However, in ferromagnets the Hall effect proportional to the magnetization—termed the anomalous Hall effect—can be driven by the relativistic spin-orbit interaction and does not require the Lorentz force (*3*). Moreover, the Hall effect of photons (*4*–*6*) and that of phonons (*7*–*9*) have been already predicted and experimentally observed. However, the Hall effect of magnons, which is relevant to spin-current electronics, has presented an experimental challenge.

We report the magnetic and thermal-transport properties of an insulating collinear ferromagnet $Lu_2V_2O_7$ with a pyrochlore structure. Figure 1A shows the vanadium sublattice in $Lu_2V_2O_7$, which is composed of corner-sharing tetrahedra. This structure can be viewed as a stacking of alternating Kagomé and triangular lattices along the [111] direction. Spin-polarized neutron diffraction suggests that the orbitals of the *d* electron are ordered so that they all point to the center of mass of the *V* tetrahedron (*10*); calculations have shown that a virtual hopping process to the high-energy state stabilizes the ferromagnetic order of the *V* spin in this orbital-ordered state (*10*). In the pyrochlore structure, because the midpoint between any two apices of a tetrahedron is not an inversion symmetry center, there is a nonzero Dzyaloshinskii-Moriya (DM) interaction

$$H_{\mathrm{DM}} = \sum_{\langle ij \rangle} \vec{D}_{ij} \cdot (\vec{S}_i \times \vec{S}_j)$$

where $\vec{D}_{ij}$ and $\vec{S}_i$ are, respectively, the DM vector between the *i* and *j* sites and the *V* spin moment at site *i*. As shown in Fig. 1B, the DM vector $\vec{D}_{ij}$ is perpendicular to the vanadium bond and parallel to the surface of the cube indicated by gray lines, according to the crystal symmetry. Even starting from the perfectly collinear ferromagnetic ground-state spin configuration, the DM interaction affects the spin wave and gives rise to the thermal Hall effect as discussed below.

The magnetic, electric, and thermal properties of $Lu_2V_2O_7$ are illustrated in Fig. 2. The spontaneous magnetization *M* emerges below Curie temperature $T_C = 70$ K (Fig. 2A). Figure 2B shows the magnetization curves along various magnetic field directions at 5 K. The magnetization saturates at relatively low field (less than 1 T), and the saturated magnetization is isotropic and almost coincides with 1 bohr magneton (μ_B), indicating the collinear ferromagnetic state with spin $S = {}^1/_2$ above the saturation field. The resistivity increases rapidly with decreasing temperature *T* (Fig. 2C). The longitudinal thermal conductivity (*11*) monotonically falls with decreasing temperature (Fig. 2D). The magnitude is small as compared with usual insulators but comparable with similar orbital-ordered materials (*12*). According to the Wiedemann-Franz law, the electric contribution of thermal conductivity is less than 10^{-5} W/K m below 100 K. Therefore, the heat current is carried only by phonons and magnons in this temperature region. From the analysis of the magnetic field variation of the thermal conductivity (*13*), we estimate the mean free paths of phonons and magnons (l_{ph} and l_{mag}, respectively) at 20 K as $l_{\mathrm{ph}} = 3.5$ nm and $l_{\mathrm{mag}} = 3.6$ nm. Because the obtained l_{ph} and l_{mag} are much larger than the *V*-*V* distance (0.35 nm), the Bloch waves of phonons and magnons are well defined at least at 20 K.

The thermal Hall effect (the Righi-Leduc effect) is usually induced by the deflection of elec-

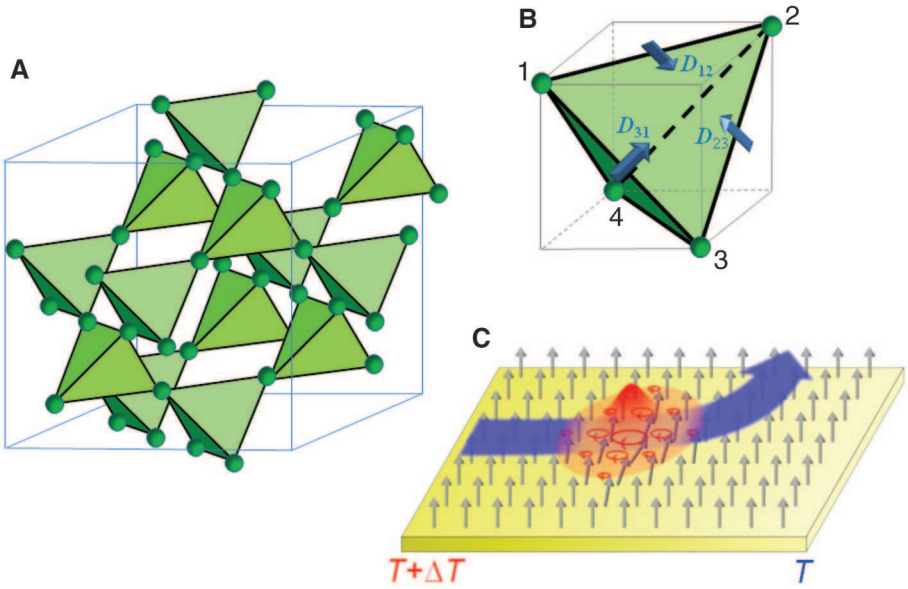

Fig. 1. The crystal structure of $Lu_2V_2O_7$ and the magnon Hall effect. (**A**) The *V* sublattice of $Lu_2V_2O_7$, which is composed of corner-sharing tetrahedra. (**B**) The direction of the Dzyaloshinskii-Moriya vector $\vec{D}_{ij}$ on each bond of the tetrahedron. The Dzyaloshinskii-Moriya interaction $\vec{D}_{ij} \cdot (\vec{S}_i \times \vec{S}_j)$ acts between the *i* and *j* sites. (**C**) The magnon Hall effect. A wave packet of magnon (a quantum of spin precession) moving from the hot to the cold side is deflected by the Dzyaloshinskii-Moriya interaction playing the role of a vector potential.

[1]Department of Applied Physics, University of Tokyo, Tokyo 113-8656, Japan. [2]Multiferroics Project, Exploratory Research for Advanced Technology, Japan Science and Technology Agency, care of Department of Applied Physics, University of Tokyo, Tokyo 113-8656, Japan. [3]Kavli Institute for Theoretical Physics, University of California, Santa Barbara, CA 93106, USA. [4]Cross-Correlated Materials Research Group and Correlated Electron Research Group, Advanced Science Institute, RIKEN, Wako 351-0198, Japan.

*To whom correspondence should be addressed. E-mail: onose@ap.t.u-tokyo.ac.jp

tronic heat current by the magnetic field in metallic materials. Because the heat current in the present material is carried only by phonons and magnons and not by charge-carriers, any observed thermal Hall conductivity would provide evidence for the Hall effect of phonons and/or magnons. Our measurements of the thermal Hall conductivity are presented in Fig. 3. Below $T_C = 70$ K, the signal is well resolved, whereas it is quite small above 80 K. The magnitude of the thermal Hall conductivity has a maximum at around 50 K. Similar to the magnetization, the thermal Hall conductivity steeply increases and saturates in the low–magnetic field region. Thus, what is presently observed in the heat transport is not the normal Hall effect proportional to the magnetic field strength but the anomalous (spontaneous) Hall effect affected by the spontaneous magnetization. However, the thermal Hall conductivity gradually decreases with magnetic field after saturation in the low-temperature region; this can be explained by the magnon gap induced by the magnetic field as discussed below. Figure 4A shows the temperature dependence of the spontaneous thermal Hall conductivity (the thermal Hall conductivity just above the saturation field) for magnetic field ∥ [100], [110], and [111]; it is independent of the field direction within the error bars.

The thermal Hall effect caused by phonons has been reported in $Tb_3Ga_5O_{12}$ (*7*) and explained by the spin-phonon interaction (*8*, *9*). The intrinsic mechanism in (*8*) does not depend on the magnon population. The mean free path of phonons is expected to increase with magnetic field as a consequence of reduced scattering by magnetic fluctuations. Therefore, our observation of the decrease of the thermal Hall conductivity in the high-field region cannot be explained in terms of the phonon mechanism. On the other hand, the reduction of the magnon population, as reflected by the behavior of the specific heat under the magnetic field (*13*), will diminish the magnon contribution of the thermal Hall conductivity. In the mechanism based on the scattering of phonons by spins (*9*), the thermal Hall angle κ_{xy}/κ_{xx} is anticipated to be proportional to the magnetization, such as in the case of $Tb_3Ga_5O_{12}$ (*7*). For $Lu_2V_2O_7$, κ_{xy} steeply decreases with increasing temperature around T_C, faster than the magnetization decreases (Fig. 4B), which contradicts the scenario of the phonon Hall effect. On the other hand, magnons propagate in terms of the exchange interaction (Eq. 3), and therefore the magnon picture cannot be valid in the magnetic field–induced spin-polarized state above T_C. Hence, the temperature dependence can be explained in terms of the magnon Hall effect.

We next turn to the quantitative calculation of the thermal Hall effect in $Lu_2V_2O_7$. This material

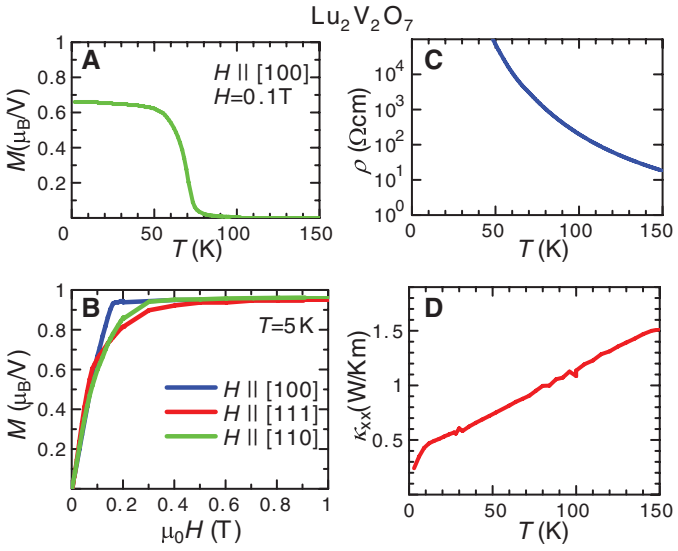

Fig. 2. Magnetic, electric, and thermal properties of $Lu_2V_2O_7$. (**A**) Temperature dependence of magnetization at the magnetic field $H = 0.1$T along the [100] direction. (**B**) Magnetization curves at $T = 5$ K for H ∥ [100], H ∥ [110], and H ∥ [111]. (**C**) Temperature variation of resistivity ρ. (**D**) Temperature variation of longitudinal thermal conductivity κ_{xx}.

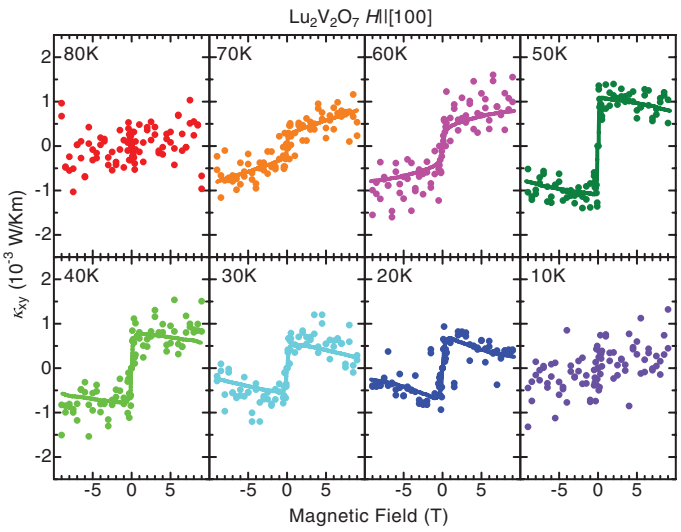

Fig. 3. Magnetic field variation of the thermal Hall conductivity of $Lu_2V_2O_7$ at various temperatures. The magnetic field is applied along the [100] direction. The solid lines are guides to the eye.

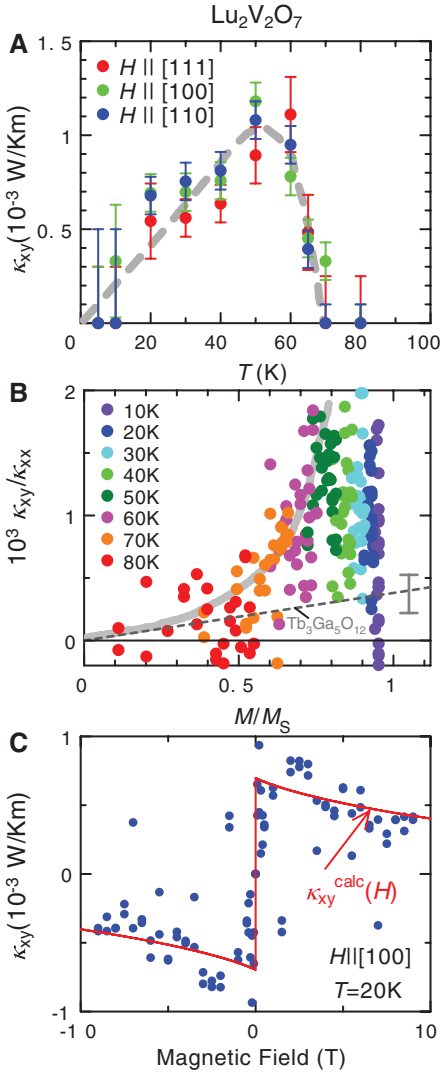

Fig. 4. (**A**) Temperature dependence of the spontaneous thermal Hall conductivity (the thermal Hall conductivity just above the saturation field) for H ∥ [100], H ∥ [110], and H ∥ [111]. The thick dashed line is a guide to the eye. (**B**) The thermal Hall angle κ_{xy}/κ_{xx} plotted against the magnetization (M). For $Tb_3Ga_5O_{12}$ (dashed line), the value of κ_{xy}/κ_{xx} divided by the magnetic field H is taken from (*7*), and the magnetic susceptibility (M/H) is estimated from the magnetization curves in (*18*). The thick solid line is a guide to the eye. (**C**) Magnetic field variation of the thermal Hall conductivity at 20 K for H ∥ [100]. The red solid line indicates the magnetic field dependence given by the theory (Eq. 4) that is based on the Dzyaloshinskii-Moriya interaction.

is a ferromagnetic Mott-insulator, and the spin-1/2 V^{4+} ions form a pyrochlore lattice (Fig. 1A). The effective spin Hamiltonian describing this system is given by

$$H_{\text{eff}} = \sum_{\langle ij \rangle} \left[-J\vec{S}_i \cdot \vec{S}_j + \vec{D}_{ij} \cdot (\vec{S}_i \times \vec{S}_j) \right] - g\mu_B \vec{H} \cdot \sum_i \vec{S}_i \quad (1)$$

where $-J$ is the nearest-neighbor ferromagnetic exchange, and the last term is the Zeeman coupling with an external field $\vec{H}$. The DM interaction does not disturb the perfect ferromagnetic alignment of the spins along the direction of a weak external magnetic field $\vec{H}$ because the sum of the DM vectors on the bonds sharing the same site is zero. Because we are interested in the low-temperature regime $T \ll T_C$, the interactions between magnons are neglected. Therefore, we consider the Bloch state of a single magnon

$$|\vec{k}\rangle = \frac{1}{\sqrt{N}} \sum_i e^{i\vec{k} \cdot \vec{R}_i} |i\rangle \quad (2)$$

where in state $|i\rangle$ the spin at site i is pointing opposite the $\vec{H}$ direction with all the other spins aligned with the $\vec{H}$ direction. The matrix element corresponding to the transfer of magnons reads as

$$\langle i| -J\vec{S}_i \cdot \vec{S}_j + \vec{D}_{ij} \cdot (\vec{S}_i \times \vec{S}_j) |j\rangle = \langle i| -\frac{J}{2}(S_i^+ S_j^- + S_i^- S_j^+) + \frac{iD_{ij}}{2}(S_i^+ S_j^- - S_i^- S_j^+) |j\rangle = -\frac{\tilde{J}}{2} e^{i\phi_{ij}} \quad (3)$$

where $S^{\pm}$ is the operator that increases or decreases the spin component along the direction $\vec{n} = (n_x, n_y, n_z) = \vec{H}/|\vec{H}|$, $D_{ij} = \vec{D}_{ij} \cdot \vec{n}$, and $\tilde{J}e^{i\phi_{ij}} = J + iD_{ij}$. Thus, the DM interaction acts as a vector potential ϕ_{ij} and serves as the "orbital magnetic field" for the propagation of magnons. The spin-wave Hamiltonian becomes just a tight-binding Hamiltonian on a pyrochlore lattice with phase factors. Thanks to the different types of loops in the unit cell of the pyrochlore lattice, the orbital magnetic field avoids the cancellation and gives rise to the Hall effect (*14*).

The formula for the thermal Hall conductivity $\kappa_{\alpha\beta}$ of the magnon system was derived in (*14*). In the low-temperature region, the dominant contribution to $\kappa_{\alpha\beta}$ comes from the lowest magnon band and small k because of the Bose distribution function. Retaining only the first-order terms in the DM interaction, the analytic expression for the anomalous thermal Hall conductivity due to magnons is obtained as (*13*)

$$\kappa_{\alpha\beta}(H,T) = \Phi_{\alpha\beta} \frac{k_B^2 T}{\pi^{3/2}\hbar a} \left(2 + \frac{g\mu_B H}{2JS}\right)^2 \times \sqrt{\frac{k_B T}{2JS}} \text{Li}_{5/2}\left[\exp\left(-\frac{g\mu_B H}{k_B T}\right)\right] \quad (4)$$

with the polylogarithm $\text{Li}_n(z)$ given by $\text{Li}_n(z) = \sum_{k=1}^{\infty} \frac{z^k}{k^n}$. Here, a is the lattice constant, and $\Phi_{\alpha\beta} = -\varepsilon_{\alpha\beta\gamma} n_\gamma D/(8\sqrt{2}J)$ with the totally antisymmetric tensor $\varepsilon_{\alpha\beta\gamma}$, and $D = |\vec{D}_{ij}|$. In Fig. 4C, we show the fitting of the data at $T = 20$ K to this expression with $JS = 8D_s/a^2$, where D_s is the spin stiffness constant obtained from the analysis of specific heat shown in (*13*). Therefore, the only parameter is the ratio of DM interaction strength D to the exchange coupling J. The agreement between experiment and theory is obtained for $D/J = 0.32$; this is a reasonable value for transition-metal oxides. In the spinel-type antiferromagnet $CdCr_2O_4$, for example, D/J has been estimated as 0.19 from the measured pitch of the spiral spin structure and ab initio calculations (*15*); this is of the same order of magnitude as our result.

We have observed the magnon Hall effect in the ferromagnetic insulator $Lu_2V_2O_7$. Other than the spontaneous spin current relevant to electronic polarization (*16*), the magnon spin current in insulating materials has rarely been discussed (*17*). The observation of the Hall effect of the magnon spin current may lead to applications of spin transport in magnetic insulators.

References and Notes

1. S. Maekawa, *Concepts in Spin Electronics* (Oxford Science Publication, Oxford, 2006), and references therein.
2. Y. K. Kato, R. C. Myers, A. C. Gossard, D. D. Awschalom, *Science* **306**, 1910 (2004).
3. N. Nagaosa, J. Sinova, S. Onoda, A. H. MacDonald, N. P. Ong, *Rev. Mod. Phys.* **82**, 1539 (2010).
4. G. L. J. A. Rikken, B. A. van Tiggelen, *Nature* **381**, 54 (1996).
5. M. Onoda, S. Murakami, N. Nagaosa, *Phys. Rev. Lett.* **93**, 083901 (2004).
6. O. Hosten, P. Kwiat, *Science* **319**, 787 (2008).
7. C. Strohm, G. L. J. A. Rikken, P. Wyder, *Phys. Rev. Lett.* **95**, 155901 (2005).
8. L. Sheng, D. N. Sheng, C. S. Ting, *Phys. Rev. Lett.* **96**, 155901 (2006).
9. Y. Kagan, L. A. Maksimov, *Phys. Rev. Lett.* **100**, 145902 (2008).
10. H. Ichikawa *et al.*, *J. Phys. Soc. Jpn.* **74**, 1020 (2005).
11. H. D. Zhou *et al.*, *Phys. Rev. B* **77**, 020411(R) (2008).
12. J.-G. Cheng, Y. Sui, J.-S. Zhou, J. B. Goodenough, W. H. Su, *Phys. Rev. Lett.* **101**, 087205 (2008).
13. Materials and methods are available as supporting material on *Science* Online.
14. H. Katsura, N. Nagaosa, P. A. Lee, *Phys. Rev. Lett.* **104**, 066403 (2010).
15. G.-W. Chern, C. J. Fennie, O. Tchernyshyov, *Phys. Rev. B* **74**, 060405(R) (2006).
16. H. Katsura, N. Nagaosa, A. V. Balatsky, *Phys. Rev. Lett.* **95**, 057205 (2005).
17. S. Fujimoto, *Phys. Rev. Lett.* **103**, 047203 (2009).
18. M. Guillot, A. Marchand, V. Nekvasil, F. Tcheou, *J. Phys. C Solid State Phys.* **18**, 3547 (1985).

19. The authors thank C. Terakura for the design of Fig. 1C and P. A. Lee, S. Fujimoto, and T. Arima for fruitful discussion. This work is supported by a Grant-in-Aid for Scientific Research (nos. 17071007, 17071005, 19048008, 19048015, 19684011, 20046004, 20340086, 21244053, and 22014003) from the Ministry of Education, Culture, Sports, Science and Technology of Japan and by the Funding Program for World-Leading Innovative R&D on Science and Technology (FIRST), Japan.

Supporting Online Material

www.sciencemag.org/cgi/content/full/329/5989/297/DC1
Materials and Methods
Figs. S1 to S3
References

12 February 2010; accepted 21 May 2010
10.1126/science.1188260

Single-Crystal X-ray Structure of 1,3-Dimethylcyclobutadiene by Confinement in a Crystalline Matrix

Yves-Marie Legrand, Arie van der Lee, Mihail Barboiu*

Cyclobutadiene (CBD), the smallest cyclic hydrocarbon bearing conjugated double bonds, has long intrigued chemists on account of its strained geometry and electronic instability, but the parent compound and its unperturbed derivatives have thus far eluded crystallographic characterization. In this work, we immobilize a precursor, 4,6-dimethyl-α-pyrone, in a guanidinium-sulfonate-calixarene (G_4C) crystalline network that confines the guest through a combination of CH-π and hydrogen-bond interactions. Ultraviolet irradiation of the crystals transforms the entrapped 4,6-dimethyl-α-pyrone into a 4,6-dimethyl-β-lactone Dewar intermediate that is sufficiently stable under the confined conditions at 175 kelvin to allow a conventional structure determination by x-ray diffraction. Further irradiation pushes the reaction to completion, enabling the structure determination of 1,3-dimethylcyclobutadiene Me_2CBD. Our data support experimental observation of square-planar (Me_2CBD^S) and rectangular-bent (Me_2CBD^R) geometries in the G_4C host matrix. The hydrogen-bonded, dissociated carbon dioxide coproduct interacts more strongly with Me_2CBD^S than with Me_2CBD^R.

Cyclobutadiene (CBD)—an unsaturated molecular ring of four carbon atoms, each capped by a single hydrogen atom—has intrigued chemists for the better part of a century (*1*–*8*). There is tremendous geometric strain associated with squeezing olefinic carbons down